# Auto-Focusing UWB Array Radar Imaging of a Target in Unknown Motion using Muller and Buffington Metrics and Cross-Range Blurriness

*Takuya Sakamoto\*[1], Toru Sato[1], Pascal Aubry[2], and Alexander Yarovoy[2]*

[1]Graduate School of Informatics, Kyoto University,
Yoshida-Honmachi, Sakyo-ku, Kyoto, 606-8501, Japan,
t-sakamo@i.kyoto-u.ac.jp, tsato@kuee.kyoto-u.ac.jp

[2]Microwave Sensing, Signals and Systems (MS3), Delft University of Technology,
Mekelweg 4, 2628 CD Delft, the Netherlands
p.j.aubry@tudelft.nl, a.yarovoy@tudelft.nl

## Abstract

We propose two target speed estimation methods for an ultra-wideband radar imaging system. The system consists of array antennas scanning while a target is moving. The proposed methods use the Muller and Buffington sharpness metric and cross-range blurriness of radar images to estimate the target speed, and compensate for the estimated motion to generate focused images automatically. The proposed methods are applied to the measurement of a knife, handgun and mannequin on an electrically-controlled moving stage. Measurement results showed that both the proposed methods can estimate target speeds, but with different accuracies. It was also confirmed that the proposed methods can generate high-quality images for moving targets with unknown speeds.

## 1. Introduction

Many conventional ultra wideband (UWB) imaging systems assume that a target is stationary while measurements are taken [1, 2]. For these systems, neglecting target motion during measurement results in blurred images. Therefore, it is crucial to develop an auto-focusing radar imaging algorithm for a target in unknown motion. Our previous study [3] proposed an auto-focusing radar imaging method using an image sharpness metric. Another approach is to use the head of a human target as a reference to estimate the speed. However, comparison of these methods has not been reported. In this study, we investigate the accuracy of these methods by applying them to three different targets: a knife, handgun and a mannequin.

## 2. System Model

The measurement system consists of a transmitter and a receiver positioned in the $z = 0$ plane in the direction of the $x$ axis at a fixed separation given by $2d$. The midpoint between the transmitter and receiver is labeled $(X, Y, 0)$, which means the transmitting and receiving antennas are located at $(X-d, Y, 0)$ and $(X+d, Y, 0)$, respectively. The transmitter-receiver pair scans at discrete intervals across a region of the $z = 0$ plane. Figure 1 shows the system setup assumed in this study. Given the antenna midpoint $(X, Y, 0)$, the signal received is labeled $s(X, Y, Z)$, where $Z = ct/2$. Here, $c$ is the speed of the electromagnetic wave and $t$ is the time interval between transmission and reception.
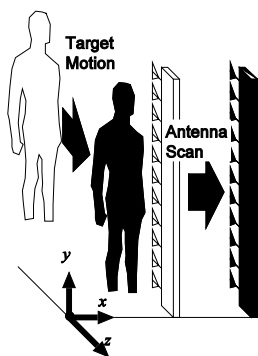


**Figure 1: Assumed system model with a target in motion and array antennas.**

## 3. Imaging using the Inverse Scattering Transform and Revised Range Point Migration

We developed a fast imaging algorithm using the bi-static inverse boundary transform (bi-static IBST) that is a reversible transform between radar signals and radar images [4]. The first step in imaging using the bi-static IBST is the extraction of signal peaks that exceeds a threshold $T_s$. These peaks are indexed as $(X_i, Y_i, Z_i)$ for ($i = 1, 2, \cdots, N$). The corresponding amplitudes of these peaks are denoted $s_i = s(X_i, Y_i, Z_i)$. Let us assume that these points are easily connected sequentially to form multiple curved surfaces $Z(X, Y)$. This function and its derivative are used in imaging with the bi-static IBST:

$$x = X - \frac{2Z^3 Z_X}{Z^2 - d^2 + \sqrt{(Z^2 - d^2)^2 + 4d^2 Z^2 Z_X^2}},$$

$$y = Y + Z_Y \left\{ d^2 (x - X)^2 - Z^4 \right\} / Z^3,$$

$$z = \sqrt{Z^2 - d^2 - (y - Y)^2 - \frac{(Z^2 - d^2)(x - X)^2}{Z^2}}$$

$$\tag{1}$$

where for simplicity $Z_X = \partial Z / \partial X$ and $Z_Y = \partial Z / \partial Y$. To obtain stable derivatives $Z_X$ and $Z_Y$, we introduced the revised range point migration (RRPM) method [4], which is known to be fast and robust even for complicated shapes in a noisy scenario. The RRPM method estimates a derivative $Z_X = \tan(\theta_i)$, where $\theta_i$ is calculated as:

$$\theta_i = \frac{\sum_{j \neq i, Y_j = Y_i} w_{i,j} \tan^{-1} \left( \frac{Z_i - Z_j}{X_i - X_j} \right)}{\sum_{j \neq i Y_j = Y_i} w_{i,j}}.$$

$$\tag{2}$$

The weighting coefficient $w_{i,j}$ in Eq. (2) is defined so that it has a large value if the $i$-th and $j$-th peaks are close to each other in terms of the target range and antenna position. This weight determines the contributing strength of the $j$-th signal peak in calculating the derivative at the $i$-th peak. In a similar way, we can estimate $Z_Y$. Finally, these derivatives are substituted into Eq. (1) to obtain the target images. The combination of the RRPM method and the bistatic-IBST is known to be computationally fast; the study in [4] showed the RRPM method was 170 times faster than conventional diffraction stack migration under similar conditions.

## 4. Muller and Buffington Sharpness Metric and Cross-Range Blurriness Metric

The image obtained with a correctly assumed speed is well-focused, which can be evaluated using two different metrics introduced in this section. The methods we propose produce multiple images corresponding to various assumed speeds, from which the optimum metric gives an estimate of the speed. It is essential to use the fast imaging technique with bi-static IBST and RRPM for calculating these metrics because the imaging is repeated many times for various assumed speeds; this process can be unpractically time-consuming if conventional methods are used instead.

The Muller and Buffington (MB) sharpness metric [5] was originally introduced to evaluate the focus quality of optical images for astronomical observations. In this study we apply this metric to three-dimensional radar images. The $q$–th order MB sharpness metric is calculated as:

$$h_q = \frac{1}{M} \sum_{m=1}^{M} I_m^q, \cdot$$

$$\tag{3}$$

where $I_m$ is the $m$-th pixel or voxel of the image, and $M$ is the total number of voxels in the three-dimensional radar image, and the order $q > 2$ is a constant that is set to $q = 4$ in this study. If the image is well focused, the MB sharpness metric has a large value that can be exploited to estimate the target speed. The MB sharpness works well, especially if the target is approximated as a collection of points.

Next, we propose another metric to measure the cross-range blurriness of a radar image. Assuming that the method is applied to a human target, this metric uses only the part of a radar image that is likely to contain a head if the target is a human. First, we estimate the head position of an image by taking the largest peak of the vertical profile of the RRPM image. Because we do not yet know the exact target speed, we assume a stationary target to produce the image in this process. Next, the image sharpness is evaluated using the horizontal image profile at the estimated head height. The image blurriness $b$ is then defined from the mean and central moments. If the image is focused, the blurriness is reduced; the actual target speed minimizes the value. Note that this method can work for non-human targets such as a knife and handgun although they do not have a 'head', because the actual target position is simply estimated as the head position. More details about this method are found in [6].

## 5. Performance Evaluation of the Proposed Methods in Measuring Data

We applied our two proposed methods using the MB sharpness metric and cross-range blurriness, to measurements obtained from three types of targets: a metallic knife, a handgun and a metal-coated mannequin shown in Figs. 2, 3, and 4. Each of these targets was placed on a moving platform. We employed frequencies from 4.0 to 20.0 GHz for the gun and knife, and 5.0 to 25.0 GHz for the mannequin. The antenna spacing was 5.5 cm, scanned at 1.0 cm intervals over an area $75.0 \times 75.0$ cm in the $x$–$y$ plane. While the antennas scanned from left to right, the target moved in the $-z$ direction over a distance of 38.0 cm, corresponding to a target speed of 1.0 m/s, assuming a total measurement time of 0.38 s. The RRPM method extracted 15 peaks for each antenna position. We set $\sigma_X = \sigma_Y = 0.8$ cm, $\sigma_Z = 0.3$ cm and $\sigma_\theta = \pi/100$. The $i$-th target image point ($x_i$, $y_i$, $z_i$) was weighted with amplitude $|s_i|$ to generate a three-dimensional image.

Figures 5, 6 and 7 show the MB sharpness metric and cross-range blurriness for the knife, handgun and mannequin, respectively. The MB sharpness metric and cross-range blurriness are plotted as dashed black and red solid lines and give the estimates of target speed. The estimated target speeds for a knife using the MB sharpness metric and cross-range blurriness are 1.04 m/s and 0.99 m/s, giving 4 and 1% relative errors. The estimated speeds for a handgun are 0.97 and 1.05 m/s with 3 and 5% errors. We see the MB sharpness metric curve in Fig. 6 is wider than that in Fig. 5, which means that the knife has a simpler shape than the handgun, which matches the MB sharpness condition. For a mannequin, the estimated speeds are 0.89 and 0.95 m/s, giving 11 and 5% errors. The MB sharpness metric gives a large error in this case, because a mannequin is difficult to approximate as a point target. In contrast, the cross-range blurriness maintains its accuracy within an acceptable range. Figure 8, 9 and 10 show the 3-D images generated using the MB sharpness metric for a knife and handgun, and the cross-range blurriness for a mannequin. It is confirmed that the shapes of targets are clearly imaged.

## 6. Conclusions

In this study, we compared two different target speed estimation methods by applying them to measurement data for three targets: a knife, handgun and mannequin. The comparison showed that the MB sharpness metric can estimate accurate target speeds for relatively small targets, whereas the cross-range blurriness is effective for all targets including the mannequin and other small targets. This result implies that the suitable method must be appropriately chosen depending on the possible target. Important future work is to investigate the performance of the methods for an actual human target.

## 7. References

1. T. Counts, A. C. Gurbuz, W. R. Scott Jr., J. H. McClellan, and K. Kim, "Multistatic Ground-Penetrating Radar Experiments," *IEEE T. Geosci. Rem. Sens.,* vol. 45, no. 8, Aug. 2007, pp. 2544–2553. 2008.

2. Y. Yang and A. E. Fathy, "Development and Implementation of a Real-Time See-Through-Wall Radar System Based on FPGA," *IEEE T. Geosci. Rem. Sens.,* vol. 47, no. 5, May 2009, pp. 1270–1280.

3. T. Sakamoto, T. Sato, P. Aubry, and A. Yarovoy, "Target Speed Estimation using Revised Range Point Migration for Ultra Wideband Radar Imaging," *P. Euro. C. Anten. Propag.*, April 2013.

4. T. Sakamoto, T. G. Savelyev, P. J. Aubry and A. G. Yarovoy, "Revised Range Point Migration Method for Rapid 3-D Imaging with UWB Radar," *Proc. 2012 IEEE Int. S. Anten. Propag. and USNC-URSI Nat. Radio Sci. Mtg,* 508.2, July 2012.

5. R. A. Muller and A. Buffington, "Real-Time Correction of Atmospherically Degraded Telescope Images through Image Sharpening," *J. Opt. Soc. Amer.,* vol. 64, no. 9, Sep. 1974, pp. 1200-1210.

6. T. Sakamoto, T. Sato, P. Aubry, and A. Yarovoy, "Target Speed Estimation using Revised Range Point Migration for Ultra Wideband Radar Imaging," *Proc. the 5th European Conference on Anten. and Propag.*, Apr. 2014 (in press).

Figure 2: A metallic knife used in our measurement.



Figure 3: A handgun used in our measurement.
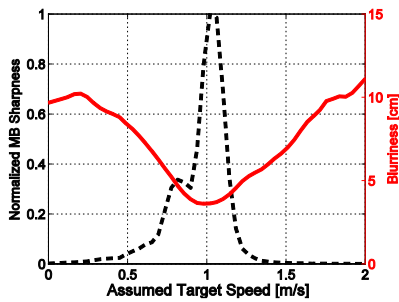


Figure 4: A mannequin used in our measurement.



Figure 5: 3-D MB sharpness metric (black) and cross-range blurriness (red) for a knife. Actual speed is 1.0 m/s.
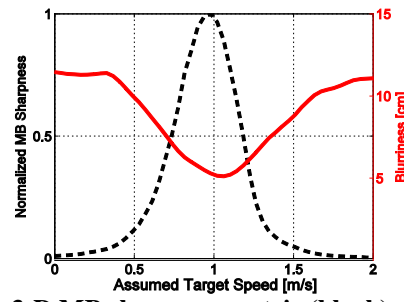


Figure 6: 3-D MB sharpness metric (black) and cross-range blurriness (red) for a handgun. Actual speed is 1.0 m/s.
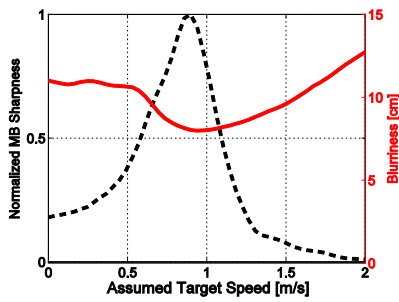


Figure 7: 3-D MB sharpness metric (black) and cross-range blurriness (red) for a mannequin. Actual speed is 1.0 m/s.
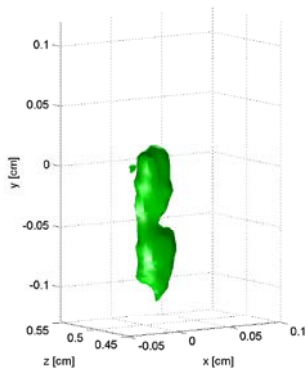


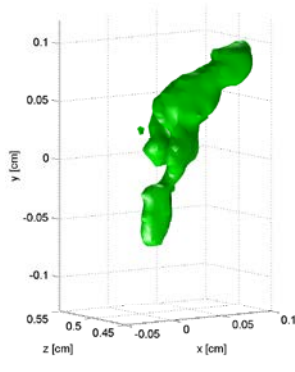Figure 8: An image generated using the proposed method for the knife.



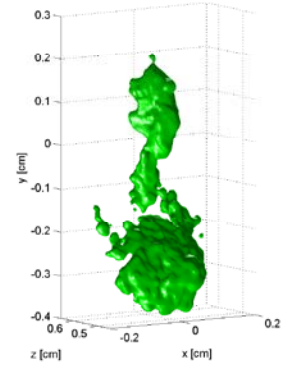Figure 9: An image generated using the proposed method for the handgun.



Figure 10: An image generated using the proposed method for the mannequin.